Local-density-derived semiempirical nonlocal pseudopotentials for InP with applications to large quantum dots

Huaxiang Fu and Alex Zunger
National Renewable Energy Laboratory, Golden, Colorado 80401
(Received 5 August 1996)

In the same way that *atomic* calculations have been used previously to extract *bare* ionic pseudopotentials, self-consistent *bulk* calculations can be used to construct *screened* atomic pseudopotentials. We use such a method to construct screened nonlocal atomic pseudopotentials for InP. A series of bulk, local-density-approximation (LDA) calculations are performed on a few InP crystal structures, covering a range of unit-cell volumes, to produce bulk potentials $\{V_{\rm LDA}(\mathbf{G})\}$. By solving a set of linear equations, we extract from these crystalline potentials the corresponding screened *atomic* ''spherical LDA'' (SLDA) potentials $v^{\alpha}_{\rm SLDA}(|\mathbf{q}|)$ for sites α=In or P. In combination with the nonlocal part of the usual LDA pseudopotentials, these SLDA potentials give band structures and wave functions that are virtually indistinguishable from the self-consistent LDA results for bulk InP. In the next step, we apply linear changes to the local SLDA potentials (while keeping the nonlocal potentials at their LDA values), to fit the band structures to *experiment*. Interestingly, this removal of LDA eigenvalue errors requires only small and subtle changes in the potential—mostly an upshift in the region near the cation core, with *nearly no change at the bond center*. Furthermore, the linear changes to the SLDA potentials result mostly in an upshift of the conduction bands with little effect on the valence bands. Because only small changes in the potential suffice to fit the bands to experimental results, the wave functions remain virtually unchanged relative to those in the original LDA calculation. Hence, we obtain semiempirical pseudopotentials which can produce *ab initio* LDA-quality wave functions with experimentally measured band structures, effective masses, and deformation potentials. The potentials obtained here were deposited on an FTP site and can be used by interested readers. Since the resulting pseudopotentials are ''soft'' (with small high-momentum components), they can be applied within a plane-wave basis in combination with a Gaussian correction to large systems for which LDA calculations are prohibitively expensive. As an illustration, we apply our InP screened atomic pseudopotentials to calculate quantum size effects on the band gaps of InP dots with sizes up to 700 atoms. Good agreement is found between the theoretical and the experimental band gaps. Fitting the calculated band gaps E_g (in unit of eV) versus the effective dot sizes D (in unit of Å) gives $E_g = 1.45 + 37.295/D^{1.16}$. This prediction differs significantly from the quadratic size dependence $D^{-2.0}$ expected from simple effective-mass theory. [S0163-1829(97)05203-X]

I. INTRODUCTION

Significant interest has recently arisen in the optical and transport properties of semiconductor quantum structures[1–4]—dots, wires, wells, and films—with typical linear dimensions of 20–100 Å. A description of the electronic properties of such 10^3–10^4 atom structures using first-principles methods[5] pertinent to bulk solids[6,7] is currently prohibitive. Furthermore, it has recently[8,9] been shown that the continuum-type effective-mass-based methods[10] may sometimes be insufficient to describe such ''small'' structures. An efficient, intermediate approach was recently proposed:[11,12] one first extracts an approximately transferable screened atomic pseudopotential from self-consistent first-principles electronic structure calculations on a series of bulk solids,[13] and then uses it to define the potential of a nanostructure.[11,12] The ensuing nanostructure Schrödinger equation is then solved using a fast direct diagonalization method in a plane-wave basis.[11] This approach is much faster than traditional self-consistent first-principles methods[5] used for bulk solids[14] in that: (i) the Schrödinger equation is solved but once, and (ii) an efficient diagonalization method providing energy levels in a fixed ''energy window'' is available and appropriate.[11] Unlike effective-mass-based approaches,[10] the method based on screened atomic pseudopotential allows us to treat explicitly the atomistic character of the nanostructure as well as surface effects, while permitting multiband and intervalley coupling. Unlike tight-binding methods,[15,16] the current method uses *explicit* and variationally flexible basis functions, thus permitting direct comparison of wave functions with local density approximation (LDA) studies when available. Note, however, that unlike LDA approaches, the current method provides only electronic structure information (levels, transition probabilities, wave functions) but no ground-state properties (e.g., equilibrium geometries), which have to be assumed at the outset.

The present method requires the knowledge of accurate and transferable screened atomic pseudopotentials. While the traditional ''empirical pseudopotential method'' [17] (EPM) does provide atomic pseudopotentials that reproduce the measured band structures of prototype bulk solids, the ensuing wave functions and deformation potentials are not constrained by the fitting procedures, nor are these pseudopotentials available at the short reciprocal lattice vectors characterizing nanostructures whose linear dimensions are a few bulk lattice constants. Wang and Zunger[13] have recently proposed a method to extract screened atomic pseudopotentials from first-principles LDA calculations on *bulk solids*

such that the wave functions are LDA-like while the band structures, effective masses, and deformation potentials match experiments. Here we apply this ''semiempirical pseudopotential method'' (SEPM) to both the bulk structure and nanostructures of InP.

The present work differs from our previous work[13] in several aspects:

(i) We develop and apply pseudopotentials for a new material system—bulk InP and InP quantum dots on which numerous experiments have been recently performed,[18–23] but little theoretical work is available. InP dots have been recently synthesized either as strain-induced ''self-assembled'' particles in metalorganic vapor phase epitaxy,[20,21] or as particles in colloidal solution growth.[22,23] The dot sizes range from 20 to 600 Å. Some interesting phenomena were found, e.g., the evolution of photoluminescence (PL) intensity with pressure,[18] the strong dependence of PL decay time on the photon energy,[19] the blueshift of the PL peak with the photoexcitation power, and band-gap renormalization effects.[20,21] Quantitative analyses of such experiments require a practical and reliable computational tool, which can reproduce excitation energies, wave-function information (e.g., transition probabilities), effective masses, and deformation potentials. The present method is suitable for such purposes.

(ii) We wish to understand the limitation of the SEPM. The SEPM approach[13] relies on representing the screened solid-state pseudopotential as linear combination of overlapping but *spherical* ''site potentials,'' and on system-to-system transferability. If such potentials are transferable from one structure to another, their Fourier transforms will lie on a ''universal'' potential-versus-momentum curve. We have seen previously[13] that both the spherical approximation and the transferability approximation work very well for Si and CdSe. But unlike Si and CdSe, the atomic size difference between In and P is very large, so the directional charge transfer in InP could be significant, raising questions on the suitability of the spherical approximation. Indeed, we find that there is a larger error for InP in the β-Sn structure than in the zinc-blende and rocksalt structures. We further find that the asymmetric part of the InP ''spherical LDA'' (SLDA) potentials deviates somewhat from a universal, potential-versus-momentum curve. This feature was not encountered before[13] in Si or in CdSe. This problem is analyzed and addressed here.

(iii) When moving from the SLDA to SEPM calculations for bulk InP, we find that only small changes to the atomic potentials can remove the LDA band-structure errors: most of the change occurs near the In atomic core with little change required near the In-P bond center. This explains why we can obtain experimentally consistent bands with LDA-like wave functions.

(iv) Application of the SEPM to large quantum dots requires paying special attention to the small reciprocal-lattice-vector components of the potentials, which are absent in periodic bulk solids from which the potentials are drawn. The sensitivity of the energy levels of dots to the small momentum components of the asymmetric pseudopotential is studied. Through this investigation, we find a simple and general way to determine the low-momentum components of the potentials. We also find that the slope of the SEPM potential at zero wave vector can have significant influence on the potential profile of quantum nanostructures.

The final semiempirical pseudopotentials are ''soft,'' so they can be applied within plane-wave bases to large systems for which LDA calculations are prohibitively expensive. Such soft pseudopotentials, which reproduce LDA-like wave functions with experimentally consistent orbital energies, can be useful in a large range of physical problems, including quantum dots, wires, and films. As an illustration, we apply our InP screened atomic pseudopotentials to the calculation of the band gaps of cubic InP quantum dots with sizes up to 700 atoms (effective size 26 Å). Good agreement is found between the theoretical band gaps and the experimentally measured values. At the same time, our band gap versus effective size relation is significantly different from that expected from simple effective-mass theory.

The paper is organized as follows. In Sec. II, the methodology is described. Section III gives the details of the construction of SEPM potentials. In Sec. IV, the applications to InP quantum dots are presented.

II. METHODOLOGY

In the first-principles LDA pseudopotential approach, the electronic structure of a solid is addressed by solving the LDA single-particle equation:[6]

$$\{-\tfrac{1}{2}\nabla^2+V^{\rm ps}_{\rm nonlocal}(\mathbf{r})+V_{\rm LDA}(\mathbf{r})\}\psi_i=\epsilon_i\psi_i\,. \tag{1}$$

Here, $V^{\rm ps}_{\rm nonlocal}(\mathbf{r})$ is the (angular momentum dependent) nonlocal part of the ionic pseudopotential, and $V_{\rm LDA}(\mathbf{r})=V^{\rm ps}_{\rm local}(\mathbf{r})+V_{\rm HXC}(\mathbf{r})$ contains the local ionic pseudopotential $V^{\rm ps}_{\rm local}$ as well as the screening potential $V_{\rm HXC}$ made up of the interelectron Coulomb (''Hartree''), exchange and correlation (XC) parts. Given an ionic pseudopotential $\{v^{\rm ps}_l(\mathbf{r})\}$ [we use consistently lower case $v(\mathbf{r})$ to denote ''atomic'' potentials, while capital $V(\mathbf{r})$ denotes crystalline potentials], Eq. (1) can be solved self-consistently for any crystal structure (denoted by σ) using well-established methods.[14]

Our approach for constructing screened site potentials consists of four steps:

First, we calculate self-consistently the crystalline potential $V^{(\sigma)}_{\rm LDA}(\mathbf{r})$ from Eq. (1) for a few bulk crystal structures σ (e.g., zinc blende, rocksalt, β-Sn) and a few unit cell volumes Ω_σ for each structure. We then extract the *spherical* component of the screened site-pseudopotential $v^{(\alpha,\sigma)}_{\rm SLDA}$ by solving:

$$V^{(\sigma)}_{\rm LDA}(\mathbf{r})\equiv V^{{\rm ps},(\sigma)}_{\rm local}(\mathbf{r})+V^{(\sigma)}_{\rm HXC}(\mathbf{r})\cong\sum_\alpha\sum_{R_{\alpha,\sigma}} v^{(\alpha,\sigma)}_{\rm SLDA}(|\mathbf{r}-\mathbf{R}_{\alpha,\sigma}|). \tag{2}$$

Here, α denotes the type of atom and $\mathbf{R}_{\alpha,\sigma}$ is the lattice vector to site α in structure σ. In Eq. (2), we have assumed that the crystal potential $V^{(\sigma)}_{\rm LDA}(\mathbf{r})$ is a superposition of *spherical* screened site pseudopotentials. We use the term ''SLDA'' to denote spherically approximated (S) LDA. In practice, we extract $v^{(\alpha,\sigma)}_{\rm SLDA}$ from a reciprocal space form of Eq. (2), namely,

$$V_{\mathrm{LDA}}^{(\sigma)}(\mathbf{G}) \cong \sum_{\alpha} S^{(\alpha,\sigma)}(\mathbf{G}) v_{\mathrm{SLDA}}^{(\alpha,\sigma)}(|\mathbf{G}|), \tag{3}$$

where $S^{(\alpha,\sigma)}(\mathbf{G}) = \Omega_{\sigma}^{-1} \Sigma_{\mathbf{R}_{\alpha,\sigma}} e^{i\mathbf{G}\cdot\mathbf{R}_{\alpha,\sigma}}$ is the structure factor and $\mathbf{G}$ is a reciprocal lattice vector. Note that $v_{\mathrm{SLDA}}^{(\alpha,\sigma)}$ is not a free-atom potential, but rather a solid-embedded site potential. The SLDA site potentials can be written conveniently as a symmetric part $v_{\mathrm{SLDA}}^{(+)}(|\mathbf{G}|)$ and an asymmetric part $v_{\mathrm{SLDA}}^{(-)}(|\mathbf{G}|)$:

$$v_{\mathrm{SLDA}}^{(+)}(|\mathbf{G}|) = v_{\mathrm{SLDA}}^{(\mathrm{In})}(|\mathbf{G}|) + v_{\mathrm{SLDA}}^{(\mathrm{P})}(|\mathbf{G}|), \tag{4}$$

$$v_{\mathrm{SLDA}}^{(-)}(|\mathbf{G}|) = v_{\mathrm{SLDA}}^{(\mathrm{In})}(|\mathbf{G}|) - v_{\mathrm{SLDA}}^{(\mathrm{P})}(|\mathbf{G}|). \tag{5}$$

Second, we fit $v_{\mathrm{SLDA}}^{(\alpha,\sigma)}(|\mathbf{G}|)$ extracted by inverting Eq. (3) to a set of Gaussian functions,

$$v_{\mathrm{SLDA}}^{(\alpha,\sigma)}(|\mathbf{G}|) = \sum_{i} c_i e^{-(|\mathbf{G}|-a_i)^2/b_i^2}, \tag{6}$$

where a_i, b_i, and c_i are fitting parameters. Using the SLDA potential [right-hand side of Eq. (2)] in place of $V_{\mathrm{LDA}}(\mathbf{r})$ of Eq. (1) yields energies and wave functions that are very close to LDA values. While the LDA wave functions are very useful and quite accurate, the LDA band gaps are usual, as underestimated.[24]

Thus, in the third step of our procedure, we adjust the parameters of Eq. (6) to reproduce the experimentally observed band structures. Insofar as the required changes in the SLDA potentials are small, the ensuing wave functions will still be quite close to the LDA results. This will then give near LDA-quality wave functions with realistic band structures.

In the fourth and final step, we treat the small momentum components of the pseudopotentials. These components are nonzero for quantum dots, but are not specified by band-structure calculations (or by the EPM) for extended bulk solids with small unit cells.

Since the final pseudopotential is rather smooth, a rapidly converged plane-wave expansion is possible. In fact, using the efficient diagonalization method[11] and our final semiempirical pseudopotentials, we can easily calculate the electronic structure of a ~1000-atom dot.

III. CONSTRUCTION OF THE SEPM POTENTIALS: DETAILS

A. SLDA potentials and their performance for bulk InP

A central question in the development of the SLDA potential is whether the spherical approximation of Eq. (3) is sufficiently accurate and transferable. If it is, the data points of $v_{\mathrm{SLDA}}^{(\alpha,\sigma)}(|\mathbf{G}|)$ versus wave-vector length $|\mathbf{G}|$ should fall on a single-valued ''universal'' curve for different structures σ and cell volumes Ω_{σ}. To test this, we have solved Eq. (1) self-consistently for InP in three crystal structures (zinc blende, rocksalt, and β-Sn) and three cell volumes for each structure, using first-principles pseudopotential methods.[14] We use the scalar-relativistic atomic pseudopotentials $\{v_l^{\mathrm{ps}}\}$ obtained from the procedure of Troullier and Martins,[25,26] employing the core correction[27] for In (having a large core with significant core-valence wave-function overlap) but not for the small-core P atom, where the correction is small. The exchange-correlation potential used is that of Perdew and Zunger.[24] Equation (1) was solved in a plane-wave basis with a knietic energy cutoff of 25 Ry. In all the calculations reported here, the nonlocal part of the ionic pseudopotential $V_{\mathrm{nonlocal}}^{\mathrm{ps}}(\mathbf{r})$ of Eq. (1) was obtained in a similar way to that of Ref. 28 but in numerical form, and was kept unchanged as we move from LDA to SLDA and SEPM. We use the ''small box'' implementation[13] to handle the nonlocal part of pseudopotential. This approach takes advantage of the short-range nature of nonlocal part, and uses the plane waves with large momentum to expand it in Fourier space.

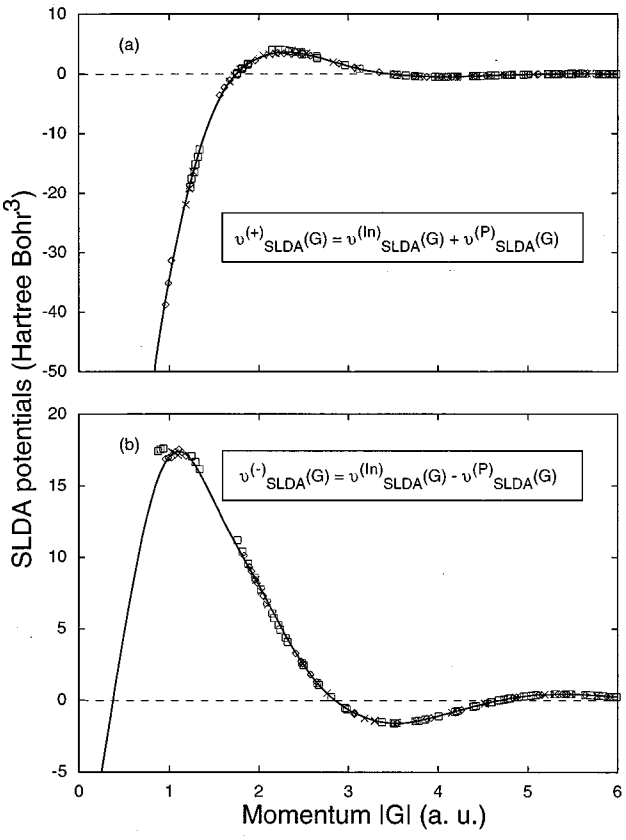

FIG. 1. Screened (local) atomic pseudopotentials $v_{\mathrm{SLDA}}(|\mathbf{G}|)$ extracted via Eq. (3) from self-consistent LDA calculations for a few bulk InP crystal structures and a few volumes each structure. (a) symmetric part $v_{\mathrm{SLDA}}^{(+)}(|\mathbf{G}|)$; (b) asymmetric part $v_{\mathrm{SLDA}}^{(-)}(|\mathbf{G}|)$. Symbols of diamond, cross and square correspond to the data for InP in zinc blende, rocksalt and β-Sn structures, respectively. Three volumes are considered for each structure. The solid lines are analytically fitted curves using Eq. (6). In the analytically fitted curves, $v_{\mathrm{SLDA}}^{(+)}(|\mathbf{G}|)$ at $\mathbf{G}=0$ is -179.32 hartree bohr^3 and $v_{\mathrm{SLDA}}^{(-)}(|\mathbf{G}|)$ at $\mathbf{G}=0$ is -14.2 hartree bohr^3.

The symbols in Fig. 1 show the LDA-derived symmetric potential $v_{\mathrm{SLDA}}^{(+)}(|\mathbf{G}|)$ versus wave vector length $|\mathbf{G}|$ as well as the asymmetric part $v_{\mathrm{SLDA}}^{(-)}(|\mathbf{G}|)$ versus $|\mathbf{G}|$. These quantities were obtained from Eq. (3) given $V_{\mathrm{SLDA}}^{(\sigma)}(\mathbf{r})$. Note that one cannot obtain the values of $v_{\mathrm{SLDA}}^{(+)}(|\mathbf{G}|)$ and $v_{\mathrm{SLDA}}^{(-)}(|\mathbf{G}|)$ at $\mathbf{G}=0$ from the inversion of bulk LDA calculation. This will be discussed later. The $v_{\mathrm{SLDA}}^{(+)}(|\mathbf{G}|)$ versus $|\mathbf{G}|$ points of Fig. 1(a) fall on a nearly universal curve for all structures and volumes, but $v_{\mathrm{SLDA}}^{(-)}(|\mathbf{G}|)$ in Fig. 1(b) is somewhat multival-

ued at the shortest bulk **G** vectors. This deviation of $v^{(-)}_{\mathrm{SLDA}}(|\mathbf{G}|)$ from a universal curve did not occur in Si [for which $v^{(-)}_{\mathrm{SLDA}}(|\mathbf{G}|)\equiv 0$] or in CdSe (see Fig. 1 in Ref. 13). We also observe that this nontransferability error is mainly reflected in the asymmetric potential $v^{(-)}_{\mathrm{SLDA}}(|\mathbf{G}|)$, while the symmetric potentials $v^{(+)}_{\mathrm{SLDA}}(|\mathbf{G}|)$ versus $|\mathbf{G}|$ fall on their respective universal curves for[13] Si, InP, and[13] CdSe. Because of the deviation of the data in Fig. 1(b) from a universal curve, several questions not met in previous work[13] arise, such as what is the effect of such deviation on the electronic structures; what is the reason for this deviation; and how can one determine the value of $v^{(-)}_{\mathrm{SLDA}}(|\mathbf{G}|)$ at $\mathbf{G}=0$.

We next investigate the effect of such small-**G** fluctuations in $v^{(-)}_{\mathrm{SLDA}}(|\mathbf{G}|)$ [Fig. 1(b)] on the *bulk* band structure. To address this, we have performed bulk band-structure calculations [via Eq. (1)] on InP using the potentials $v^{(+)}_{\mathrm{SLDA}}(|\mathbf{G}|)$ of Fig. 1(a) and $v^{(-)}_{\mathrm{SLDA}}(|\mathbf{G}|)+\delta v^{(-)}(|\mathbf{G}|)$, where $\delta v^{(-)}(|\mathbf{G}|)$ is a controlled deviation. We find that near the shortest bulk zinc-blende reciprocal lattice vector ($|\mathbf{G}|=\sqrt{3}\,2\pi/a$, where a is the lattice constant), the sensitivity $\partial\epsilon_{nk}/\partial v^{(-)}$ of the band structure ϵ_{nk} to the fluctuation $\delta v^{(-)}$ is less than 5.0×10^{-3} (in units of 1/bohr^3) for the lowest eight bands over the first Brillouin zone (BZ) for bulk InP in zinc-blende and rocksalt structures. Given that the largest scatter of $v^{(-)}_{\mathrm{SLDA}}(|\mathbf{G}|)$ in Fig. 1 is about 20 eV bohr^3, the maximum ensuing band structure error is only about 0.1 eV for zinc-blende and rocksalt structures. For the β-Sn structure, this nontransferability error increases to about 0.2 eV. Thus, the scatter in $v^{(-)}_{\mathrm{SLDA}}(|\mathbf{G}|)$ has only a small effect on *bulk* band-structure calculations.

Before we fit the SLDA data in Fig. 1 using the analytic expression in Eq. (6), we need the values of $v^{(\pm)}_{\mathrm{SLDA}}(|\mathbf{G}|)$ at $\mathbf{G}=0$. $v^{(+)}_{\mathrm{SLDA}}(|\mathbf{G}|)$ at $\mathbf{G}=0$ is obtained by fitting to the InP work function (see Appendix A). While the value of $v^{(-)}_{\mathrm{SLDA}}(|\mathbf{G}|)$ near $\mathbf{G}=0$ has no effect on bulk band structures, it could affect quantum dot levels. To investigate this effect quantitatively, we have solved Eq. (1) for an InP quantum dot, using the SLDA potential of Fig. 1 with controlled changes in $v^{(-)}_{\mathrm{SLDA}}(|\mathbf{G}|)$ at near-zero **G** values. [Details of the method used to solve Eq. (1) for dots are given below]. We allowed fluctuations of ± 10 hartree bohr^3 in the value of $v^{(-)}_{\mathrm{SLDA}}(|\mathbf{G}|)$ near $\mathbf{G}=0$. After passivating the surface dangling bonds (see below), we find that such a potential fluctuation shifts the conduction-band minimum (CBM) and valence-band maximum (VBM) eigenvalues of a 35-atom InP dot by less than 0.05 eV [so $\partial\epsilon_i/\partial v^{(-)}|_{\mathbf{G}=0}\simeq 9.0\times10^{-5}$ in units of 1/bohr^3]. We conclude that the small-**G** fluctuations in $v^{(-)}_{\mathrm{SLDA}}(|\mathbf{G}|)$ are rather inconsequential to the electronic structures of both solids and quantum dots. Since it is rather difficult to determine uniquely the precise value of $v^{(-)}_{\mathrm{SLDA}}(|\mathbf{G}|)$ near $\mathbf{G}=0$, our conclusion on the insensitivity of the energy levels to small **G** components of $v^{(-)}_{\mathrm{SLDA}}$ is significant. In fact, given this relative insensitivity, we can fix the $\mathbf{G}=0$ components of $v^{(+)}_{\mathrm{SLDA}}(|\mathbf{G}|)$ and $v^{(-)}_{\mathrm{SLDA}}(|\mathbf{G}|)$ using simple procedures, the details of which are described in Appendix A.[29] Having fixed the $\mathbf{G}=0$ components of the screened pseudopotentials, we now have an absolute energy scale in the problem. Thus, we will be able to discuss, for example, absolute energy positions of the VBM and CBM separately as a function of dot size.

We now curve fit the obtained discrete $v^{(\pm)}_{\mathrm{SLDA}}(|\mathbf{G}|)$ data points in Fig. 1 including their $\mathbf{G}=0$ limits using a convenient analytic expression—a sum of Gaussians as described in Eq. (6). The fitted curves are shown as solid lines in Fig. 1.

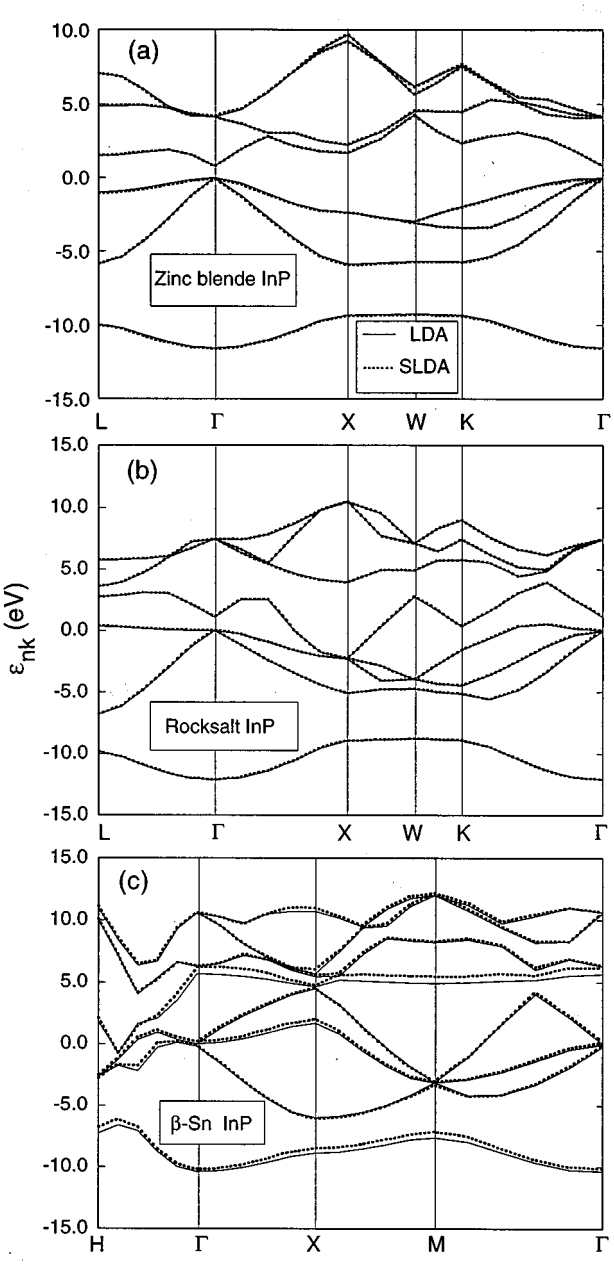

FIG. 2. Band structures calculated from LDA potentials (solid lines) and from SLDA potentials (dotted lines) for InP in different crystal structures: (a) Zinc-blende structure (lattice constant $a=11.01$ a.u.); (b) Rocksalt structure ($a=10.28$ a.u.); (c) β-Sn structure ($a=13.91$, $c=7.93$ a.u.). The lattice parameters are optimized by LDA calculations. In (a) and (b), the LDA and the SLDA band structures are nearly indistinguishable, showing that a superposition of spherical potentials is a good approximation to the LDA potential.

As a final test of the spherically approximated LDA potential, we solve Eq. (1) using the original LDA value for $V^{\mathrm{ps}}_{\mathrm{nonlocal}}(\mathbf{r})$, and the curve-fitted SLDA potential [Eq. (6)] in place of $V_{\mathrm{LDA}}(\mathbf{r})$. The resulting band structures are compared in Fig. 2 with the original (nonspherical) LDA band structures. Excellent agreement is found: the maximum BZ-

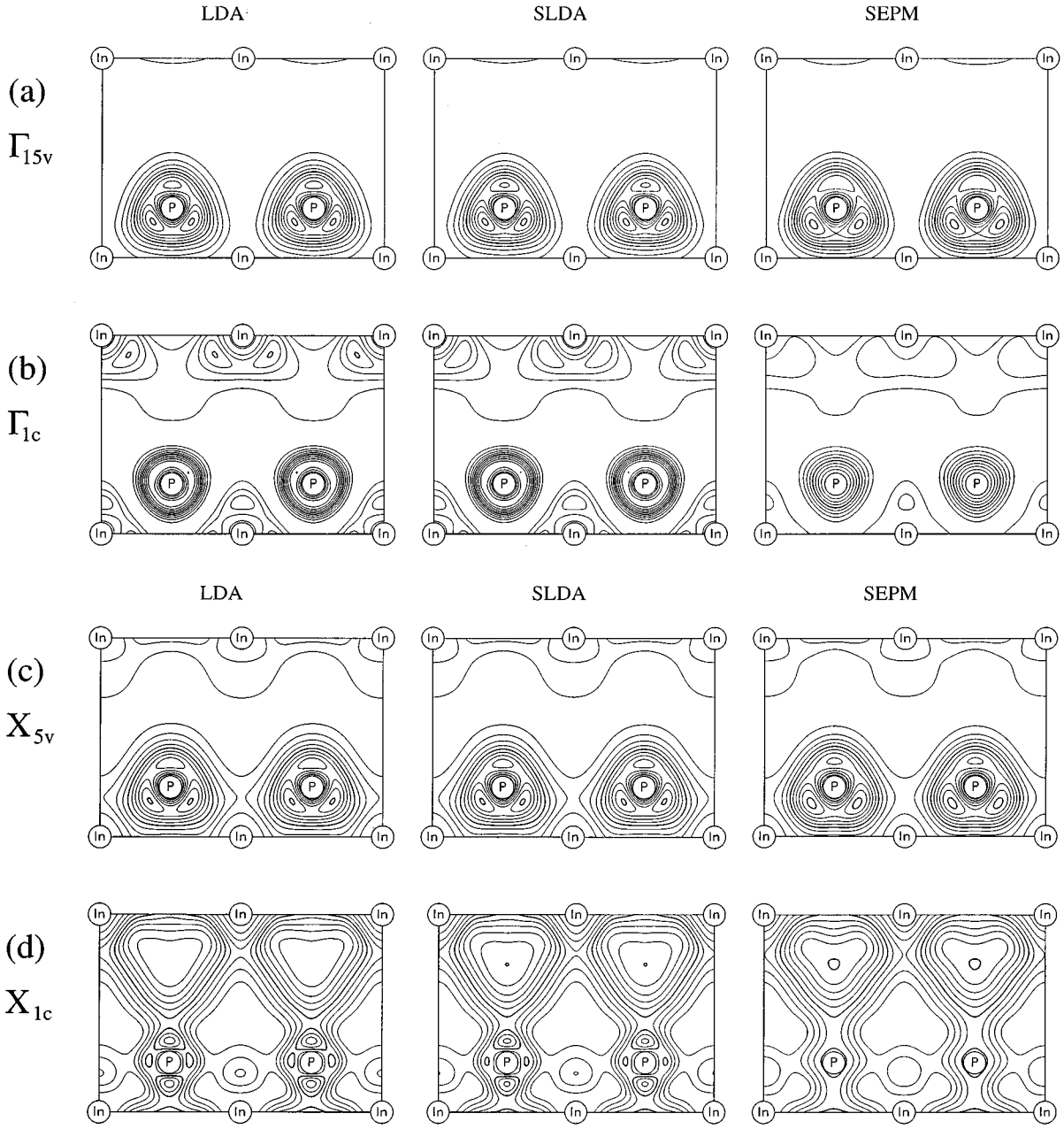

FIG. 3. Contour plots of wave-function squares on the (110) plane for the Γ_{15v}, Γ_{1c}, X_{5v}, and X_{1c} states in zinc-blende InP (lattice constant $a=11.01$ a.u.) as calculated by using LDA, SLDA, and SEPM potentials. The LDA and SLDA results are obtained using kinetic cutoff energy $E_{\text{cut}}=25$ Ry, and the SEPM results are obtained using $E_{\text{cut}}=6.8$ Ry and the Gaussian correction (Appendix B).

averaged errors between the LDA and the SLDA results are 0.07 and 0.02 eV for the lowest eight bands in zinc-blende and rocksalt InP, respectively. In the metallic β-Sn form, the error is larger: 0.35 eV for the first and fifth bands and 0.1 eV for other bands. In order to find the reason for this relatively large error, we intentionally let the fitted curve in Fig. 1(b) pass through the β-Sn data points. Application of this potential to study the band structure will result in error reflecting only the spherical approximation. We find that in the β-Sn structure the spherical approximation error is about 0.15 eV and the nontransferability error is 0.20 eV for the first and fifth bands. We attribute the relatively larger error for β-Sn structure to the large difference in the sizes of the In and P atoms, and to the low symmetry of the β-Sn structure.

We find that the LDA wave functions are also accurately reproduced by our fitted SLDA potentials. As an example, Fig. 3 compares the contour plots of the wave-function squares for the Γ_{15v}, Γ_{1c}, X_{5v}, and X_{1c} states of zinc-blende InP as calculated from the LDA and from the fitted SLDA potentials. The agreement is excellent: the LDA versus SLDA wave-function overlap is larger than 99.9%.

The first three columns in Table I[29–41] compare zinc-blende InP band energies, effective masses, and deformation potentials obtained from LDA and SLDA calculations, showing good agreement.

The good agreement between LDA and SLDA calculations persists after we reduce the kinetic cutoff energy from 25 to 6.8 Ry, while compensating for the reduced basis by

TABLE I. Energy levels at high-symmetry points, effective masses for electrons (m_e), heavy holes (m_{HH}) and light holes (m_{LH}), deformation potentials $a(\mathbf{k})$ defined as $-\partial E_g(\mathbf{k})/\partial \ln\Omega$ and work function of zinc-blende InP as calculated by LDA, SLDA, and SEPM potentials. Our assessment of the best value of the related experimental data is also listed for comparison. The energy levels, deformation potential, and work function are all in eV. The zero of the energy is at the valence-band maximum (Γ_{15v}).

Properties	LDA	SLDA	SEPM	Expt.
Γ_{1v}	−11.54	−11.50	−11.46	−11.00[a]
Γ_{1c}	0.76	0.86	1.45	1.43[b]
Γ_{15c}	4.11	4.24	4.90	4.78[c]
X_{5v}	−2.35	−2.29	−2.23	−2.0[a]
X_{1c}	1.64	1.77	2.30	2.40[d]
L_{3v}	−0.97	−0.96	−0.92	−1.00[a]
L_{1c}	1.49	1.60	1.97	2.04[e]
m_e	0.057	0.060	0.095	0.079,[f] 0.081[g]
$m_{\mathrm{HH}}(001)$	0.43	0.40	0.47	0.52,[b] 0.61[i]
$m_{\mathrm{HH}}(111)$	0.97	0.90	1.03	0.95,[j] 0.63[h]
$m_{\mathrm{LH}}(001)$	0.057	0.057	0.097	0.104,[i] 0.118[h]
$a(\Gamma)$	6.04	6.75	8.19	7.98,[k] 6.40[l]
$a(X)-a(\Gamma)$	−7.53	−6.04	−5.81	−6.82[l]
$a(L)-a(\Gamma)$	−3.18	−2.76	−3.08	−3.12[l]
Work function			5.91	5.85[m]

[a]Reference 30.
[b]Reference 31.
[c]Reference 32.
[d]Reference 33.
[e]Reference 34.
[f]Reference 35.
[g]Reference 36
.
[h]Reference 37.
[i]Reference 38.
[j]Reference 39.
[k]Reference 40.
[l]Reference 41.
[m]Reference 29.

using the ''Gaussian correction'' (GC) method[13] as described in Appendix B and in Fig. 4. The reduction of the kinetic energy cut-off can reduce significantly the computational effort for quantum nanostructures.

B. SEPM potentials and their performance for bulk InP

In the next step, we apply linear changes to the curve-fitted potentials $v^{(\pm)}_{\mathrm{SLDA}}(|\mathbf{G}|)$ [i.e., we only change the coefficients $\{c_i\}$ in Eq. (6)] so as to fit their bulk eigenvalues to the experimentally observed excitations. The obtained potential is called the SEPM potential. The required changes in the potentials are found to be small, and therefore the changes in the wave functions relative to the LDA calculation are also small.

Table I compares the band energies, effective masses, and deformation potentials obtained by using the SLDA potential and the empirically corrected potential (SEPM). In this table, the pertinent experimental results are included for comparison. We see that the SEPM achieves good accord with the pertinent experimental quantities, including the band structures at Γ, X, and L points, the effective masses and deformation potentials. The SEPM band structures of InP in zinc-blende structures are compared in Fig. 5 with the SLDA band structures. We see that, except for the upshifts of the conduction bands, the main features and trends of the whole

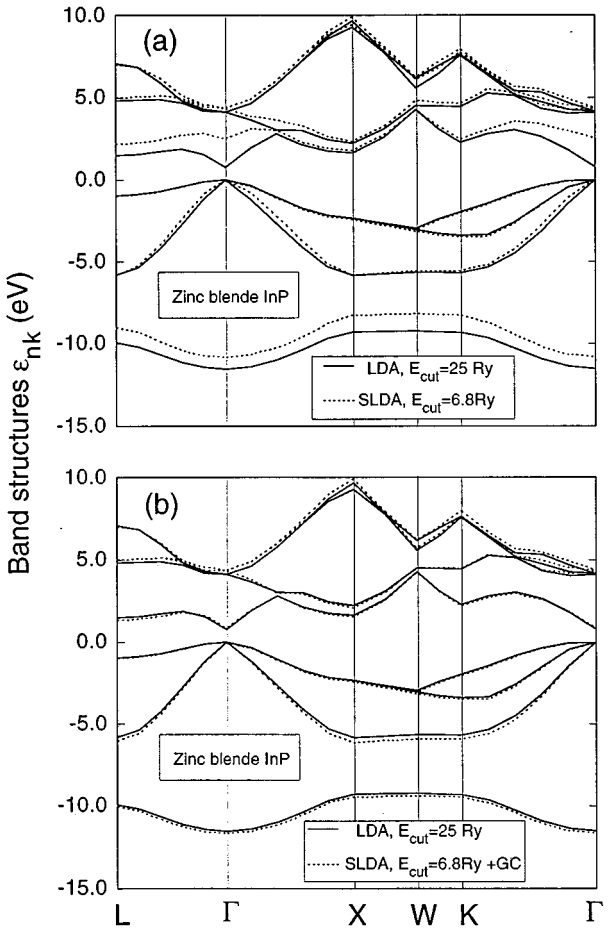

FIG. 4. (a) Band structures of InP in zinc-blende structure (a =11.01 a.u.) as calculated using LDA potentials with kinetic cutoff energy E_{cut}=25 Ry (solid lines), and as calculated by SLDA potentials with E_{cut}=6.8 Ry and without Gaussian correction (dotted lines). Note the large difference between two results. (b) Same as (a) except that dotted lines are obtained with Gaussian correction. Note the close agreement with LDA when the Gaussian correction compensates the reduced energy cutoff (Appendix B).

SEPM band structures follow those of the SLDA. The wave-function squares of SEPM calculations for some bulk states are illustrated in Fig. 3, showing good agreement with LDA and SLDA results.

C. Effects of removing the LDA error

The **G**-space SEPM potential and the shift $\Delta v = v^{(\alpha)}_{\mathrm{SEPM}} - v^{(\alpha)}_{\mathrm{SLDA}}$, needed to remove the LDA error in the band structures, are shown in Fig. 6, while Fig. 7 shows $v^{(\alpha)}_{\mathrm{SEPM}}$ and Δv in real space. There are two interesting aspects involving the effect of the removal of the LDA error:

(i) Spatial location of the LDA potential error: We see from Fig. 7 that correcting the LDA band-structure error entails an increase in the LDA potential in the core region for the In atom, and only slight changes for the P atom, while the potential at the In-P bond center does not change much. The effect of the potential increase in the core region on band structures can be readily understood: Since the atomic In s orbital energy is higher than that of the P s orbital, the location of the lowest conduction band (the antibonding state

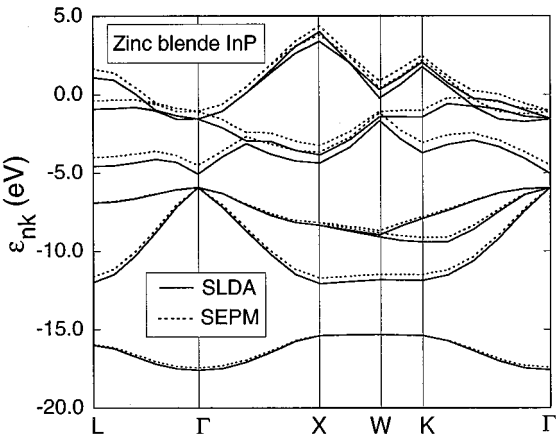

FIG. 5. The zinc-blende InP band structure calculated from SEPM (dotted lines) and from SLDA potentials (solid lines). The lattice constant is $a=11.01$ a.u. Both the SEPM and the SLDA band energies are given in absolute values. Since the VBM positions are very close to each other for LDA and SLDA bands, this figure shows that most of the LDA error is in the conduction bands.

formed from the *s* orbitals of the two atoms) is mainly determined by the atomic energy level of the In *s* orbital. The increase of the SEPM potential relative to the SLDA potential in the In core region will push up the atomic energy level

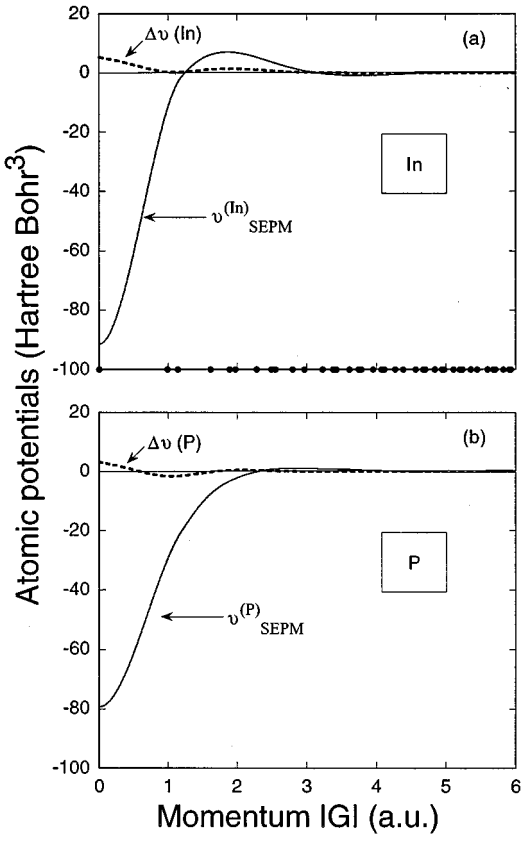

FIG. 6. The semiempirical atomic potentials $v^{(\alpha)}_{\mathrm{SEPM}}$ (solid lines) and the shift $\Delta v = v^{(\alpha)}_{\mathrm{SEPM}} - v^{(\alpha)}_{\mathrm{SEPM}}$ (dotted lines) in **G** space: (a) for In; (b) for P. Dots on the axis indicate zinc-blende reciprocal-lattice-vector lengths for bulk InP.

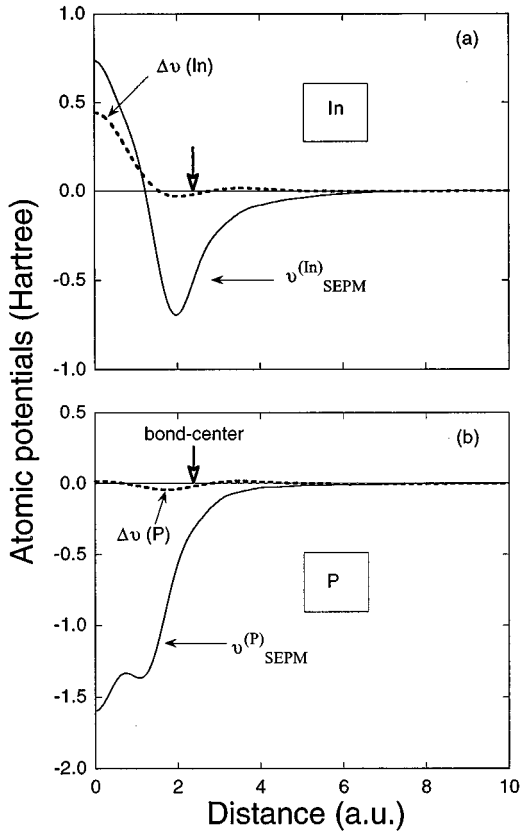

FIG. 7. The semiempirical atomic potentials $v^{(\alpha)}_{\mathrm{SEPM}}$ (in solid lines) and the shift $\Delta v = v^{(\alpha)}_{\mathrm{SEPM}} - v^{(\alpha)}_{\mathrm{SLDA}}$ (in dotted lines) in real space: (a) for In; (b) for P. The vertical arrow indicates the In-P bond center.

of the In *s* orbital, consequently raising the lowest conduction band. Due to the orthogonalization constraint, the higher conduction bands will also be pushed up as shown in Fig. 5. The valence bands bear only little change since the *p* orbital energy is not affected by shifting the In potential near the origin. Furthermore, since the potentials near the In-P bond center do not change significantly, the In-P interaction will not change much. This suggests that the wave function will not change too much either. This is borne out by the similarity of SEPM and LDA wave functions shown in Fig. 3. The fact that the error in SLDA potential is mostly in the atomic core region and is different for *s* and *p* valence electrons suggests that one could improve the SEPM fit by treating the nonlocal part of the pseudopotential also as a parametrized function. At this stage, however, we prefer not to introduce additional fitting functions.

(ii) Energy location of the LDA error: Figure 5 gives the SEPM and SLDA bands of zinc-blende InP *on an absolute scale* (i.e., the VBM's are not aligned). The comparison of SEPM band structures relative to SLDA results shows that the main effect of the removal of LDA error is to move the conduction bands up while the valence bands do not change much. This situation is similar to what was found in more elaborated *GW* calculations.[42]

D. Effect of the potential slope at G=0 on nanostructures

So far, our discussion has centered on bulk materials. Application of SEPM potentials to quantum nanostructures

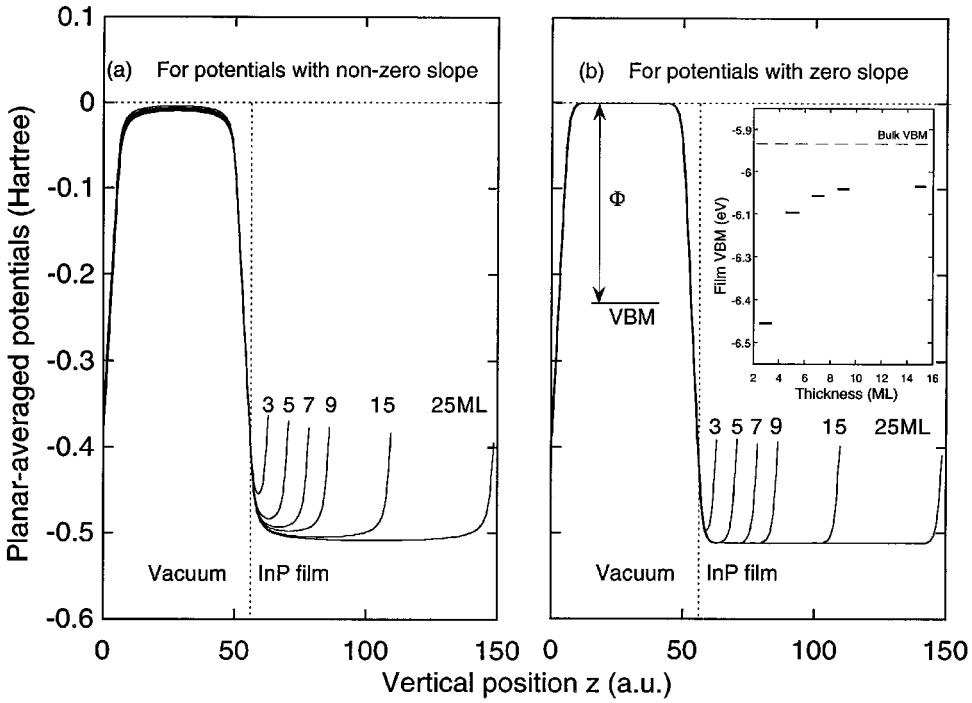

FIG. 8. Planar-averaged potentials $\bar{\bar{V}}_a(z)$ [Eq. (7)] for InP(110) films with different thickness, as calculated using: (a) SEPM potentials with nonzero slope; (b) SEPM potentials with zero slope at $\mathbf{G}=0$. The labeled numbers for each curve are the film thickness (in monolayers). The arrow in (b) indicates the theoretically fitted work function. The film VBM energies for different thicknesses are shown in the inset in (b).

(which contain reciprocal lattice vectors that are absent in the bulk) requires that the potentials should be flat near $\mathbf{G}=0$ i.e., the potential slope at $\mathbf{G}=0$ is zero. As an illustration of this point, we calculated the planar-averaged potential $\bar{\bar{V}}_a(z)$ for (110)-oriented InP films with different thicknesses, using the SEPM potentials (i) with nonzero slope and (ii) with zero slope at $\mathbf{G}=0$. Here,

$$\bar{\bar{V}}_a(z)=\frac{1}{2l}\int_{z-l}^{z+l}\bar{V}(z')dz', \tag{7}$$

where

$$\bar{V}(z)=\frac{1}{S}\int V(\mathbf{r})dx\,dy, \tag{8}$$

$$V(\mathbf{r})=\sum_{\alpha}\sum_{\mathbf{R}_i} v^{(\alpha)}_{\mathrm{SEPM}}(\mathbf{r}-\mathbf{R}_i). \tag{9}$$

In the above equations, z is the distance from one side of the supercell along the direction vertical to the film, and S is the area of cross section parallel to the film plane. l is the thickness of a single monolayer in the InP(110) film. The planar-averaged potential $\bar{\bar{V}}_a(z)$ for films with different thicknesses are shown in Fig. 8(a) for the SEPM potentials with nonzero slope, and in Fig. 8(b) for the SEPM potentials with zero slope at $\mathbf{G}=0$. It can be seen that in Fig. 8(a) the potential at the slab center has not approached the bulk value even for 15-ML-thick films while the potential in Fig. 8(b) has achieved the bulk value at the film center even for rather thin films. This $\mathbf{G}=0$ treatment has no effect on the properties of bulk InP, but is crucial for the investigation of quantum confinement effect in nanostructures such as in dots. The slopes of the SEPM potentials generated previously[13] for Si and CdSe are very close to zero too.

The final InP SEPM as well as the Si and CdSe potentials can be found on an FTP site for the interested readers.[43] They can be used in numerous applications requiring large-scale calculations.

IV. APPLICATIONS TO QUANTUM DOTS

As an illustration of the utility of our semiempirical pseudopotential, we use it to calculate the band gaps of surface-passivated InP quantum dots with different sizes. Here we discuss only the salient features of the results. A detailed description of InP quantum dot will be deferred to a future paper.

We consider InP dots containing 17, 29, 107, 259, and 712 atoms (not including the passivating atoms). The dots take cubic shape with faces oriented along the (001) and (110) planes of zinc-blende structure. Using the same density as in the bulk, the effective dot sizes are calculated by $D=(a/2)(N)^{1/3}$ where a is the lattice constant and N is the number of atoms in the dots. This gives effective sizes $D=7.49$, 8.95, 13.83, 18.57, and 26.01 Å for the dots with 17, 29, 107, 259, and 712 atoms, respectively.

We next discuss the surfaces of the dots. Previous calculations on other-material dots using the $\mathbf{k}\cdot\mathbf{p}$ theory,[44] tight-binding method,[45] or truncated crystal method[46] have ignored the existence of surfaces either by assuming infinite potential barrier or by removing the dangling bonds in the Hamiltonian matrix. Since one of our future objectives is to study surface effects on the electronic structures of dots, we

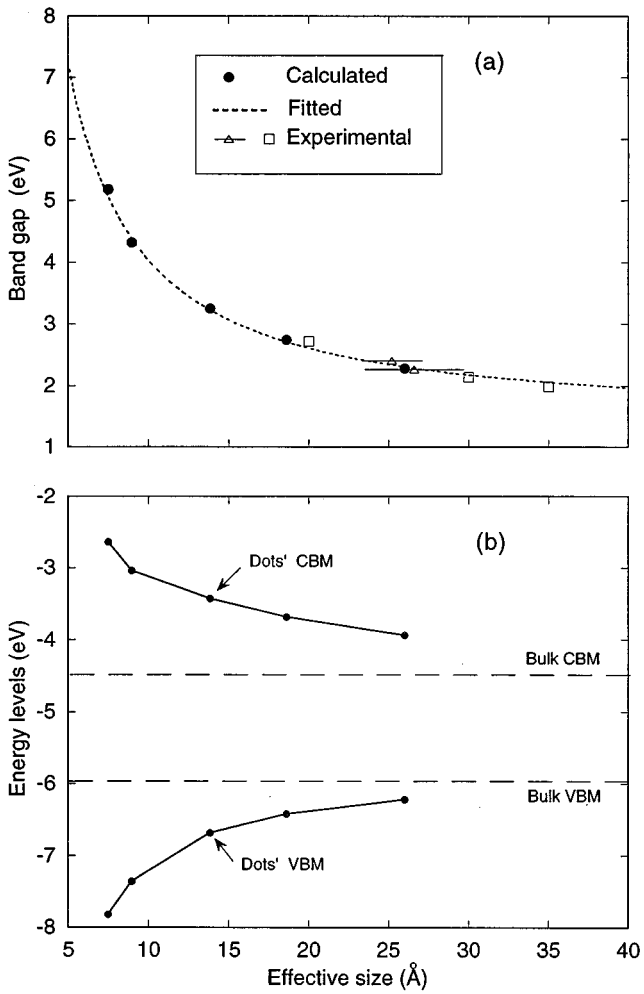

FIG. 9. (a) One-electron band gap for InP quantum dots with different sizes. Solid dots: calculated results using SEPM potentials; dash line: analytic fit of the calculated results from Eq. (11); triangle and square symbols denote, respectively, the experimental data from absorption and photoluminescence measurements (Refs. 22 and 23). For the experimental data shown here, the electron-hole Coulomb energy has been subtracted. (b) Calculated VBM and CBM levels of InP quantum dots.

include here explicit surface effects. For bare (unpassivated) dots, the atoms at the surface will most likely reconstruct. Here we model, instead, dots grown by self-assembled method[20,21] or by colloidal solution.[22,23] In both cases, the atoms at the surface are passivated chemically either by another semiconductor[20,21] or by organic molecules,[22,23] so the surface is, most likely, unreconstructed. Generally, the surface conditions of dots are different for differently prepared samples. However, based on the measurements of PL lifetime and PL efficiency, it is found that the emission originates mostly from dot-interior (''bulklike'') states, not from surface states. In recent experiments for InP dots, organic compounds and HF solution are used to passivate and etch the surface.[22,23] In these experiments, the passivation effect of organic compounds and HF at the InP dot surface is quite similar to attaching an electrostatic potential to the surface dangling bond. We thus simulate the actual passivation in dots by attaching the following fictitious pseudopotential to In-like and P-like dangling bonds:

$$u_\alpha = u_\alpha^0 \exp(-|\mathbf{r}-\mathbf{R}|^2/r_\alpha^2), \tag{10}$$

where $\mathbf{R}$ is the spatial position of the passivating atom. The parameters $\{u_\alpha^0, r_\alpha\}$ are selected so as to fit the calculated surface density of states of planar InP surfaces to LDA results or to photoemission data for surfaces.[47] This procedure was described in Ref. 11 for Si. Here we illustrate the electronic structure of InP quantum dots using the typical values: For the InP(110) surface, $u_\alpha^0 = -3.5$ hartrees and $r_\alpha = 0.9$ a.u. for surface In, and $u_\alpha^0 = -2.0$ hartrees and $r_\alpha = 1.0$ a.u. for surface P. For the InP(100) surface, $u_\alpha^0 = -1.5$ hartrees and $r_\alpha = 1.4$ a.u. for surface In, and $u_\alpha^0 = -0.5$ hartrees and $r_\alpha = 1.5$ a.u. for surface P. These values produce a band gap free of surface states for all the InP(110) and InP(001) films.[47] We point out that, after removing the surface states out of the gap, the band-edge energy levels of dots are not sensitive to the passivating potentials. We will return to this point later.

In order to solve the Schrödinger equation with many atoms, we use the folded spectrum and conjugate gradient methods,[11] allowing us to find the energy levels and wave functions of the CBM and VBM states of dots. The calculated band gaps for these dots are illustrated in Fig. 9(a) while the VBM and CBM energy levels of dots are shown in Fig. 9(b). For comparison, the available experimental data from absorption spectrum[22] and PL measurements[23] are also shown in Fig. 9(a). The experimental values are converted to one-electron band gaps by subtracting the electron-hole Coulomb energy calculated from $E_c = -3.572/\varepsilon D$ (Ref. 48). Here, E_c and the size D are both given in atomic units, and the static dielectric constant ε of InP is[49] 12.4. Figure 9(a) shows that the theoretical one-electron gaps are in good agreement with the experimental measurements. The quantum size effects on both the CBM and the VBM of dots are obvious in Fig. 9(b). Note that the energy levels in Fig. 9(b) are absolute values since our SEPM potentials are obtained by fitting the work function. Therefore, we can discuss the size effect separately for the VBM and the CBM of dots. We fitted our calculated band gaps (E_g in units of eV) versus the size of InP dots (D in units of Å) as

$$E_g = 1.45 + 37.295/D^n, \quad n = 1.16. \tag{11}$$

This analytic equation is described by the dashed line in Fig. 9(a). Not surprisingly, the value $n = 1.16$ from our atomistic calculation is very different from that found in classic effective-mass theory of $n = 2.0$.

In order to investigate the natures of the VBM and CBM of dots, we have calculated the planar-averaged wave-function square $\overline{|\psi_m|^2}$ along certain directions, where m is the energy-level index. The planar-averaged wave-function square $\overline{|\psi_m|^2}(x)$ along the x direction and $\overline{|\psi_m|^2}(z)$ along the z direction are defined as

$$\overline{|\psi_m|^2}(x) = \frac{1}{S_{yz}} \int |\psi_m(\mathbf{r})|^2 dy\, dz, \tag{12}$$

$$\overline{|\psi_m|^2}(z) = \frac{1}{S_{xy}} \int |\psi_m(\mathbf{r})|^2 dx\, dy, \tag{13}$$

where S_{yz} and S_{xy} are the cross-section areas of the plane perpendicular to the x axis and that of the plane perpendicu-

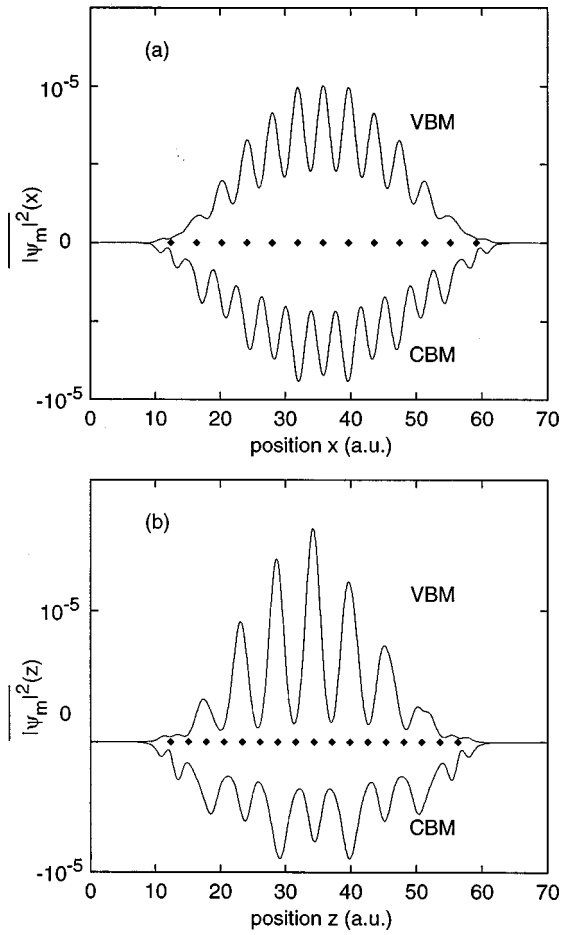

FIG. 10. (a) Planar-averaged wave-function square $\overline{|\psi_m|^2}(x)$ along the x direction. For clarity, $\overline{|\psi_m|^2}(x)$ for VBM is plotted along positive vertical axis while $\overline{|\psi_m|^2}(z)$ for CBM is plotted along negative vertical axis. The symbols along the horizontal axis indicate the atomic-layer positions. (b) Planar-averaged wave-function squares $\overline{|\psi_m|^2}(z)$ along the z direction.

lar to the z axis, respectively. For the InP dots considered here, the x, y, and z axes are along (110), (1$\bar{1}$0), and (001) directions of InP zinc-blende structure, respectively. The x and y directions are equivalent for the dots considered here. Figures 10(a) and 10(b) give, respectively, the planar-averaged wave-function squares $\overline{|\psi_m|^2}(x)$ and $\overline{|\psi_m|^2}(z)$ for the dot with 712 atoms. In this figure, symbols along the horizontal axis indicate atomic-layer positions in the dot. From Fig. 10, we can see that the wave functions of both the CBM and VBM are mostly distributed in the interior of dot, with but little amplitude at the dot surface. For such ''dot-interior'' states, changes in the passivation potential (e.g., different saturation species) cannot shift these energy levels significantly. A similar situation is found in experiments.[22,23]

In summary, we derive the semiempirical pseudopotentials for InP from *ab initio* LDA pseudopotential calculations. The obtained SEPM potentials reproduce accurately the LDA wave functions and the experimentally observed band structures, effective mass, and deformation potential. Since it is soft, the SEPM potential can be used efficiently in large-scale quantum nanostructure calculations using plane-wave bases. This is illustrated here for the band gaps of InP quantum dots with different sizes, showing a good agreement with the experimental results.

ACKNOWLEDGMENTS

We would like to thank A. Franceschetti, S. Froyen, L. W. Wang, S. H. Wei, and S. B. Zhang for their helpful discussions. We also thank A. Williamson for carefully reading the manuscript. This work was supported by the U.S. Department of Energy, OER-BES, under Grant No. DE-AC36-83CH10093.

APPENDIX A: DETERMINATION OF $v^{(+)}_{\mathrm{SLDA}}(|\mathbf{G}|)$ AND $v^{(-)}_{\mathrm{SLDA}}(|\mathbf{G}|)$ AT $\mathbf{G}=0$

When one calculates the electronic structures of quantum dots using plane-wave bases and supercells, the knowledge of $v^{(+)}_{\mathrm{SLDA}}(|\mathbf{G}|)$ and $v^{(-)}_{\mathrm{SLDA}}(|\mathbf{G}|)$ at small $\mathbf{G}$ is necessary. In this Appendix, the procedures to determine $v^{(+)}_{\mathrm{SLDA}}(|\mathbf{G}|)$ and $v^{(-)}_{\mathrm{SLDA}}(|\mathbf{G}|)$ at $\mathbf{G}=0$ are described.

$v^{(+)}_{\mathrm{SLDA}}(|\mathbf{G}|)$ at $\mathbf{G}=0$ is determined by noting that changes in this quantity shift rigidly the whole bulk band structure. We thus require that the work function of thick InP film (the negative of the eigenvalue of film's VBM) equals its observed, orientationally averaged value of[29] 5.85 eV. This gives $v^{(+)}_{\mathrm{SLDA}}(\mathbf{G}=0)=-179.32$ hartree bohr^3 for InP with lattice constant $a=11.01$ a.u. Using this value, the theoretical work function of thick InP film is 5.91 eV. Due to the quantum confinement effect, the VBM energy level of the film changes with the film thickness. The calculated VBM for a series of (110) InP slabs embedded in vacuum is shown in the inset of Fig. 8(b). For the thickest slab shown in the figure, we can see a work function close to the measured value.

The determination of $v^{(-)}_{\mathrm{SLDA}}(|\mathbf{G}|)$ at $\mathbf{G}=0$ is more complicated. One may consider obtaining $v^{(-)}_{\mathrm{SLDA}}(|\mathbf{G}|)$ at small $\mathbf{G}$ by computing $V_{\mathrm{LDA}}(\mathbf{G})$ in Eq. (1) for long period superlattices of pure InP with different levels of strain, e.g., $(\mathrm{InP})_n/(\text{strained InP})_n$. Since the potential of long period superlattices contains small $\mathbf{G}$ components, one could extrapolate the superlattice $V_{\mathrm{LDA}}(\mathbf{G})$ to $\mathbf{G}=0$. However, we found that the superlattice structure factors $S(\mathbf{G})$ in Eq. (3) for the small $\mathbf{G}$ vectors are very small due to the structural similarity of the superlattice to the bulk. The small $S(\mathbf{G})$ values lead to a significant scatter and noise in the calculated $v^{(-)}_{\mathrm{SLDA}}(|\mathbf{G}|)$ at small $\mathbf{G}$.

Based on the fact (described in Sec. III) that both the VBM and CBM levels of quantum dots are rather insensitive to $v^{(-)}_{\mathrm{SLDA}}(|\mathbf{G}|)$ at small $\mathbf{G}$, we use a simple approach to estimate this value. Having fixed $v^{(+)}_{\mathrm{SLDA}}(|\mathbf{G}|)$ at $\mathbf{G}=0$ by fitting the work function and having fitted analytically $v^{(+)}_{\mathrm{SLDA}}(|\mathbf{G}|)$ using Eq. (6), we now have this function in the whole $\mathbf{G}$ space. We can thus Fourier transform $v^{(+)}_{\mathrm{SLDA}}(|\mathbf{G}|)$ to $v^{(+)}_{\mathrm{SLDA}}(r)$. We next need to separate in $v^{(+)}_{\mathrm{SLDA}}(r)$ the components due to In and due to P so that the $v^{(-)}_{\mathrm{SLDA}}(r)$ could be calculated. To do this, we assume that the In and P solid-state potentials $v^{\mathrm{In}}_{\mathrm{SLDA}}(r)$ and $v^{\mathrm{P}}_{\mathrm{SLDA}}(r)$ can be written as a product of screened free-atom potential $\tilde{v}^{\alpha}\equiv v^{\alpha}_{\mathrm{ion}}+v_{\mathrm{HXC}}$ and a screening factor $\alpha_i e^{-r/\beta_i}$, i.e.,

$$v_{\mathrm{SLDA}}^{(+)}(r)=[\alpha_1 e^{-r/\beta_1}]\tilde{v}^{\mathrm{In}}(r)+[\alpha_2 e^{-r/\beta_2}]\tilde{v}^{\mathrm{P}}(r). \tag{A1}$$

We now fit the right-hand side of Eq. (A1) to the left-hand side using α_1, β_1, α_2, and β_2 as fitting parameters. After determining α_1, β_1, α_2, and β_2 from Eq. (A1), we obtain $v_{\mathrm{SLDA}}^{(-)}(r)$ in real space from

$$v_{\mathrm{SLDA}}^{(-)}(r)=[\alpha_1 e^{-r/\beta_1}]\tilde{v}^{\mathrm{In}}(r)-[\alpha_2 e^{-r/\beta_2}]\tilde{v}^{\mathrm{P}}(r). \tag{A2}$$

Fourier transforming this $v_{\mathrm{SLDA}}^{(-)}(r)$ gives $v_{\mathrm{SLDA}}^{(-)}(\mathbf{G}=0)$. For zinc-blende InP at lattice constant $a=11.01$ a.u., we find $v_{\mathrm{SLDA}}^{(-)}(\mathbf{G}=0)=-14.2$ hartree bohr.[3]

APPENDIX B: GAUSSIAN CORRECTION TO SMALL BASIS SET CUTOFF

A known shortcoming of a plane-wave basis set band-structure calculation is that the number of basis functions is usually quite large, especially when we deal with large systems such as quantum dots or long period superlattices. Here, we adopt a method to reduce the cutoff energy.

Generally, when small cutoff energy is used, the band structures are poorly converged. This is illustrated in Fig. 4(a), showing the band structures of bulk InP in the zinc-blende structures (with lattice constant being 11.01 a.u.) as calculated with a converged basis of 25-Ry cutoff and a small basis of 6.8-Ry cutoff. It can be seen that while the p bands (e.g., the top three valence bands) are described quite well, the s bands (e.g., the lowest conduction band and the lowest valence band) are affected strongly by the reduction in basis set size. In order to correct this kind of difference, an additional Gaussian-type potential $q_i e^{-|r-\mathbf{R}_\alpha/d_i|^2}$ is placed at each atomic site $\mathbf{R}_\alpha$ for both In and P atoms. Here, q_i and d_i are determined by minimizing the difference between two kinds of band structures (i.e., converged LDA and Gaussian corrected SLDA with a small basis). We find $q=-4.27$ hartrees and $d=0.7$ bohr for In, and $q=-2.53$ hartrees and $d=0.7$ bohr for P. Figure 4(b) shows the band structures for zinc-blende InP corresponding to 6.8-Ry cutoff energy with the Gaussian correction in comparison with those corresponding to 25-Ry cutoff energy. It can be seen that, using the Gaussian-type correction potential leads to the band structures that are very similar to the pure plane-wave converged results. Using the same Gaussian parameters, for other crystal structures—rocksalt and β-Sn—we find errors of $\leqslant 0.2$ eV. We use the same Gaussian corrections in all of our calculations for InP quantum dots.

[1] See, for example, *Microcrystalline and Nanocrystalline Semiconductors*, edited by R. W. Collins, C. C. Tsai, M. Hiros, F. Koch, and L. E. Brus, MRS Symposium Proceedings No. 358 (Materials Research Society, Boston, 1994).

[2] *Light Emission from Novel Silicon Materials*, edited by Y. Kanemitsu, M. Kondo, and K. Takeda (The Physical Society of Japan, Tokyo, 1994).

[3] *Optical Phenomena in Semiconductor Structures of Reduced Dimensionality*, Vol. 248 of *NATO Advanced Study Institute Series E: Applied Sciences*, edited by D. J. Lockwood and A. Pinczuk (Kluwer Academic, Dordrecht, 1993).

[4] L. W. Wang and A. Zunger, in *Nanocrystalline Semiconductor Materials*, edited by P. V. Kamat and D. Meisel (Elsevier Science, Amsterdam, 1996); A. D. Yoffe, Adv. Phys. **42**, 173 (1993).

[5] F. Buda, J. Kohanoff, and M. Parrinello, Phys. Rev. Lett. **69**, 1272 (1992).

[6] W. Kohn and L. J. Sham, Phys. Rev. **140**, A1133 (1965); J. Perdew and A. Zunger, Phys. Rev. B **23**, 5048 (1981).

[7] R. M. Dreizler and E. K. U. Gross, *Density Functional Theory* (Springer-Verlag, Berlin, 1990).

[8] D. M. Wood and A. Zunger, Phys. Rev. B **53**, 7949 (1996).

[9] S. B. Zhang, C. Y. Yeh, and A. Zunger, Phys. Rev. B **48**, 11 204 (1993).

[10] O. Kane, J. Phys. Chem. Solids **1/2**, 83 (1956); G. Bastard, *Wave Mechanics Applied to Semiconductor Heterostructures* (Les Edition de Physique, Les Ulis, 1988).

[11] L. W. Wang and A. Zunger, J. Chem. Phys. **100**, 2394 (1994); J. Phys. Chem. **94**, 2158 (1994); Phys. Rev. B **53**, 9579 (1996).

[12] K. A. Mäder, L. W. Wang, and A. Zunger, Phys. Rev. Lett. **74**, 2555 (1995); K. A. Mäder, and A. Zunger, Phys. Rev. B **50**, 17 393 (1994); A. Franceschetti and A. Zunger, Phys. Rev. B **52**, 14 664 (1995).

[13] L. W. Wang and A. Zunger, Phys. Rev. B **51**, 17 398 (1995).

[14] J. Ihm, A. Zunger, and M. L. Cohen, J. Phys. C **12**, 4409 (1979).

[15] N. A. Hill and K. B. Whaley, Phys. Rev. Lett. **75**, 1130 (1995).

[16] G. D. Sanders and Y. C. Chang, Phys. Rev. B **45**, 9202 (1992).

[17] M. L. Cohen and T. K. Bergstresser, Phys. Rev. **141**, 789 (1966); J. R. Chelikowsky and M. L. Cohen, Phys. Rev. B **14**, 556 (1976); M. L. Cohen and J. R. Chelikowsky, *Electronic Structure and Optical Properties of Semiconductors* (Springer-Verlag, Berlin, 1989).

[18] C. Ulrich, S. Ves, A. R. Goni, A. Kurtenbach, S. Syassen, and K. Eberl, Phys. Rev. B **52**, 12 212 (1995).

[19] A. A. Yamaguchi, J. Ahopelto, K. Nishi, A. Usui, H. Akiyama, and H. Sakaki, *Gallium Arsenide and Related Compounds*, edited by T. Ikegami, F. Hasegawai, and Y. Takeda (IOP, Bristol, UK, 1992), p. 341.

[20] P. Castrillo, D. Hessman, M. E. Pistol, S. Anand, N. Carlsson, W. Seifert, and L. Samuelson, Appl. Phys. Lett. **67**, 1905 (1995).

[21] S. Anand, N. Carlsson, M. E. Pistol, L. E. Samuelson, and W. Serfert, Appl. Phys. Lett. **67**, 3016 (1995).

[22] O. I. Micic, C. J. Curtis, K. M. Jones, J. R. Sprague, and A. J. Nozik, J. Phys. Chem. **98**, 4966 (1994).

[23] O. I. Micic, J. R. Sprague, Z. H. Lu, and A. J. Nozik, Appl. Phys. Lett. **68**, 3152 (1996); O. I. Micic (private communication).

[24] J. Perdew and A. Zunger, Phys. Rev. B **23**, 5048 (1981).

[25] N. Troullier and J. L. Martins, Phys. Rev. B **43**, 8861 (1991).

[26] In generating atomic pseudopotentials, we use the atomic configurations In:$5s^2 5p^{0.5} 5d^{0.1}$ and P:$3s^2 3p^{2.5} 3d^{0.1}$ while the matching-point radii are 1.98, 2.30, and 3.80 a.u. for s, p, and d, respectively in In, and 1.45, 1.60, and 3.80 a.u. for s, p, and d, respectively in P. Tests on different configurations and radii show only slight changes (within 10^{-3} eV) in the total energy.

[27] S. G. Louie, S. Froyen, and M. L. Cohen, Phys. Rev. B **26**, 1738 (1982).

[28] D. R. Hamann, M. Schluter, and C. Chiang, Phys. Rev. Lett. **43**, 1494 (1979).
[29] J. van Laar, A. Huijser, and T. L. van Rooy, J. Vac. Sci. Technol. **14**, 894 (1977).
[30] L. Ley and R. A. Pollak, Phys. Rev. B **9**, 600 (1974).
[31] Z. Hang, H. Shen, and F. H. Pollak, Solid State Commun. **36**, 15 (1990).
[32] P. Lautenschlager, M. Garriga, and M. Cardona, Phys. Rev. B **36**, 4813 (1987).
[33] S. W. Tozer, D. J. Wolford, J. A. Bradley, D. Bour, and G. B. Stringfellow, *Proceedings of the 19th ICPS, Warsaw, Poland*, edited by W. Zawadski (Institute of Physics, Polish Academy of Sciences, 1988), p. 881.
[34] L. W. James, J. P. Van Dyke, F. Herman, and D. M. Chang, Phys. Rev. B **1**, 3988 (1970).
[35] P. Rochon and E. Fortin, Phys. Rev. B **12**, 5803 (1975).
[36] J. M. Chamberlain, J. Phys. C **4**, L38 (1971).
[37] J. Leotin, R. Barbaste, S. Askenazy, M. S. Skolnick, R. A. Stradling, and J. Tuchendler, Solid State Commun. **15**, 693 (1974).
[38] D. Bimberg, K. Hess, N. O. Lipari, J. U. Fischbach, and M. Altarelli, Physica B & C **89**, 139 (1977).
[39] P. Lawaetz, Phys. Rev. B **4**, 3460 (1971).
[40] G. D. Pitt, Solid, State Commun. **8**, 1119 (1980).
[41] R. Zallen and W. Paul, Phys. Rev. **155**, 703 (1967).
[42] M. S. Hybertsen and S. G. Louie, Phys. Rev. Lett. **55**, 1418 (1985).
[43] ftp to ftp.nrel.gov as ''anonymous,'' change directory to pub/sst-out/InP.SEPM, and download all the files.
[44] Al. L. Efros and A. V. Rodina, Phys. Rev. B **47**, 10 005 (1993).
[45] P. E. Lippens and M. Lannoo, Phys. Rev. B **39**, 10 935 (1989).
[46] M. V. Rama Krishna and R. A. Friesner, Phys. Rev. Lett. **67**, 629 (1991).
[47] T. Chasse, G. Neuhold, and K. Horn, Surf. Sci. **331-333**, 511 (1995); A. Tulke and H. Luth, *ibid*. **211/212**, 1001 (1989); A. Huijser, J. v. Laar, and T. L. v. Rooy, *ibid.* **62**, 472 (1977).
[48] L. E. Brus, J. Phys. Chem. **90**, 2555 (1986).
[49] K. Seeger, Appl. Phys. Lett. **54**, 1268 (1989).